Long-range corrected time-dependent density functional study on fluorescence of 4,4′-dimethylaminobenzonitrile

Mahito Chiba
Department of Applied Chemistry, School of Engineering, The University of Tokyo, Tokyo 113-8656, Japan

Takao Tsuneda
Department of Quantum Engineering and Systems Science, School of Engineering, The University of Tokyo, Tokyo 113-8656, Japan

Kimihiko Hirao
Department of Applied Chemistry, School of Engineering, The University of Tokyo, Tokyo 113-8656, Japan

(Received 7 November 2006; accepted 30 November 2006; published online 17 January 2007)

Dual fluorescence of 4,4′-dimethylaminobenzonitrile (DMABN) was theoretically investigated on the basis of long-range corrected time-dependent density functional theory. Excited-state geometry optimization states and single-point energy calculations with and without solvent effect were carried out. It has been explained that DMABN emits dual fluorescence only in polar solvents through locally excited (LE) and charge transfer (CT) states. It was, however, concluded from this study that although the main spectrum of dual fluorescence in acetonitrile solvent is clearly due to twisted intramolecular CT fluorescence, small secondary fluorescence in acetonitrile may also emanate from CT fluorescence during the DMABN twisting process. This conclusion is supported by an experimental interpretation on polarization spectroscopy. It was also found that the optimized DMABN geometries have certain wagging angles for the CT state and no wagging angle for the LE state. This may support an early experimental hypothesis that the dual fluorescence of DMABN is induced by the wagging mode due to vibronic coupling between LE and CT states. Consequently, the authors propose a fluorescence mechanism of DMABN in gas phase and in acetonitrile solvent: the main absorption proceeds to the CT state in both situations. In gas phase, single fluorescence is chiefly emitted from the LE state through the internal conversion from CT to LE states. Dual fluorescence in acetonitrile solvent may only be emitted from the CT state. © *2007 American Institute of Physics*. [DOI: 10.1063/1.2426335]

I. INTRODUCTION

4,4′-dimethylaminobenzonitrile (DMABN, Fig. 1) is one of the most well-known dual fluorescence systems. Lippert *et al.* found that DMABN emits anomalously redshifted fluorescence with secondary fluorescence in polar solvents.[1] According to Platt's notation,[2] DMABN has two types of emissions: normal ^1L_b-type and redshifted ^1L_a-type fluorescence. However, it does not emit this dual fluorescence either in the gas phase or in nonpolar solvents. It has been interpreted that DMABN only exhibits locally excited (LE) emissions with no charge transfer (CT) emissions under these conditions. In polar solvents, DMABN exhibits dual fluorescence, LE emission and CT emission.

There are many experimental investigations on the dual fluorescence mechanism.[3–10] Rotkiewicz *et al.*[3] and Grabowski *et al.*[5] suggested that twisted intramolecular charge transfer (TICT) plays a major role in dual fluorescence.[3,5] This TICT model has been the most widely accepted model so far. In this model, the initially promoted excited state descends along the slope of the potential energy surface by twisting the dimethylamino group from a planar to a perpendicular position relative to the benzonitrile group. This twisting leads to the decoupling of the dimethylamino and benzonitrile groups and induces charge transfer from the amino group to the aromatic ring. Based on time-resolved fluorescence spectra in various solvents, Kühule and coworkers proposed another model, in which planar intramolecular charge transfer (PICT) plays an important role.[6,9,10] This mechanism requires a sufficiently small energy gap between LE and CT states, which allows efficient vibronic coupling between these two states. The wagging of the amino group in this PICT mechanism induces the decoupling of the lone pair of N with the aromatic group in the LE state. However, this PICT mechanism was theoretically disputed from an energetic point of view.[11] Sobolewski and Domcke suggested another model based on rehybridization by CT.[12] In this model, CT induces the $sp \rightarrow sp^2$ rehybridization of the carbon atoms in the cyano group of DMABN. This rehybridization model has also come under suspicion in theoretical calculations.[13] Fluorescence and absorption spectra have

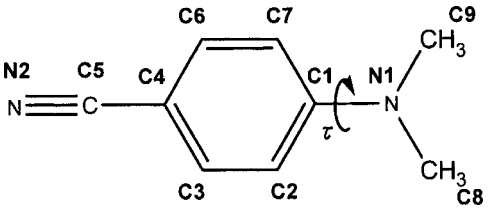

FIG. 1. The structure of DMABN.

been observed for CT and LE excitations in different solvents.[4,8] These spectra revealed that the CT state is stabilized by solvent polarity. The crystal structure of DMABN has also been observed in experiments.[14]

Many theoretical investigations have also been performed on the fluorescence of DMABN.[15–21] Theoretical calculations of this fluorescence essentially require excited-state geometry optimizations, because electronic excitations accompany the structural changes of DMABN. In conventional theoretical studies, the excited states of DMABN were investigated by single-point energy calculations with a high-level theory, e.g., *ab initio* complete-active-space second-order perturbation theory[22,23] and time-dependent density functional theory[24,25] (TDDFT), at an excited-state geometry, which was optimized by a lower-level theory, e.g., CIS and CASSCF, or at a ground state geometry, in which only the twisting angle was varied.[11–13,15–21] However, it is known that CIS and CASSCF methods often give poor geometries for excited states, because these methods essentially do not include dynamical electron correlation.[26] Such approach using a low-level theory for optimizing geometries and a high-level theory for calculating single-point energies has been widely used in equilibrium state calculations for avoiding the enormous computational timings of high-level *ab initio* calculations. This approach may be inappropriate especially for investigating excited-state dynamics. By implementing the analytical excited-state energy gradient of TDDFT,[27] Rappoport and Furche recently optimized the excited-state geometries of DMABN by TDDFT with hybrid B3LYP (Ref. 28) functional (TDB3LYP).[29] As a result, TDB3LYP gave more accurate geometries and excitation energies than those of low-level *ab initio* theories with a low computational cost equivalent to that of CIS. However, poor CT energies were found to be a major problem in TDDFT calculation. It is well known that conventional TDDFTs include hybrid. We suggest that there is a room for more theoretical investigation on the dual fluorescence of DMABN, because one of this dual fluorescence is attributed to the CT excitation as mentioned above.

Recently, it was suggested that the poor behaviors of charge transfer excitations by conventional TDDFTs are clearly solved by applying the long-range correction (LC) scheme to TDDFT formalism.[30,31] This LC scheme simply improves the long-range interaction part of generalized-gradient approximation (GGA) exchange functionals by combining with the Hartree-Fock (HF) exchange integral only for the long electron-electron distance.[32,33] The basic concept of the LC scheme is to complement the long-range exchange interaction, which is fundamentally not reproduced by any pure exchange functional of electron density,[34] in GGA functionals. In corrections for (TD)DFT,[35–37] the LC scheme may be the simplest with the least (one) parameter despite of its wide applicability. Computational effort required in LC-TDDFT calculation is almost equivalent to those of conventional TDDFT or CIS. By calculating the intramolecular CT excitation energy of ethylene-tetrafluoroethylene dimer, it was found that LC-TDDFT gives a correct behavior of charge transfer excitation energies, while conventional TDDFTs including TDB3LYP totally failed to describe this behavior.[30] This result showed that conventional TDDFTs including hybrid functionals do not contain long-range exchange interaction which is necessary for describing long-range charge transfer. Besides, the LC scheme improves the description of van der Waals interactions,[38,39] hyperpolarizabilities,[40] and so on in DFT and TDDFT calculations. Recently, we developed the analytical energy gradient of LC-TDDFT.[31] By optimizing excited-state geometries by this LC-TDDFT gradient, we found that the LC scheme is necessary in TDDFT calculations to provide accurate geometries and excitation energies especially for CT excitations.[31]

In this study, the dual fluorescence mechanism of DMABN is theoretically investigated by using the analytical excited-state energy gradient of LC-TDDFT. First, the excited-state DMABN geometries and potential energy curves are calculated for the LE and CT states with no solvent effects. The absorption energies and two different emission energies are then calculated with and without solvent effect. The corresponding oscillator strengths are also evaluated. Evaluated energies were compared with the results of experiments and conventional high-level *ab initio* theories and conventional TDDFTs. Based on these results, the fluorescence mechanism of DMABN is discussed for gas phase and acetonitrile solvent conditions in detail.

II. THEORY

A. Long-range correction scheme for exchange functional

The LC scheme modifies the long-range electron-electron interaction part of exchange functional explicitly by combining with the HF exchange integral.[32,33] In this scheme, electron repulsion operator $1/r_{12}$ is divided into short- and long-range parts by using the standard error function "erf" as

$$\frac{1}{r_{12}} = \frac{1-\mathrm{erf}(\mu r_{12})}{r_{12}} + \frac{\mathrm{erf}(\mu r_{12})}{r_{12}}, \tag{1}$$

where $r_{12}=|\boldsymbol{r}_1-\boldsymbol{r}_2|$ for coordinate vectors of electrons, $\boldsymbol{r}_1$ and $\boldsymbol{r}_2$, and μ is an adapted parameter determining the ratio of these parts. Following Eq. (1), the short-range part of exchange energy is expressed by modifying a GGA exchange functional as[32]

$$E_x^{\mathrm{sr}} = -\frac{1}{2}\sum_\sigma \int \rho_\sigma^{4/3} K_\sigma \left\{ 1 - \frac{8}{3} a_\sigma \left[\sqrt{\pi}\,\mathrm{erf}\left(\frac{1}{2a_\sigma}\right) + 2a_\sigma(b_\sigma - c_\sigma) \right] \right\} d^3r, \tag{2}$$

where ρ_σ is the density of σ-spin electrons at a spatial point $\boldsymbol{r}$, and K_σ is a GGA part of exchange functional. In Eq. (2), a_σ, b_σ, and c_σ are given as

$$a_\sigma = \frac{\mu K_\sigma^{1/2}}{6\sqrt{\pi}\rho_\sigma^{1/3}}, \tag{3}$$

$$b_\sigma = \exp\left(-\frac{1}{4a_\sigma^2}\right) - 1, \tag{4}$$

and

$$c_\sigma = 2a_\sigma^2 b_\sigma + \frac{1}{2}. \tag{5}$$

The long-range part of the exchange energy is expressed by a modified HF exchange integral,

$$E_x^{\mathrm{lr}} = -\frac{1}{2}\sum_\sigma \sum_i^{\mathrm{occ}} \sum_j^{\mathrm{occ}} \int\int \psi_{i\sigma}^*(r_1)\psi_{j\sigma}^*(r_2) \times \frac{\mathrm{erf}(\mu r_{12})}{r_{12}} \psi_{i\sigma}(r_1)\psi_{j\sigma}(r_2) d^3r_1 d^3r_2, \tag{6}$$

where $\psi_{i\sigma}$ is the ith σ-spin molecular orbital (MO). The parameter σ was determined so as to minimize the mean absolute deviation of the calculated equilibrium distances for the homonuclear diatomic molecules of the first- to third-row atoms except rare-gas atoms with the 6-311++G(2d,2p) basis set. For BOP (Refs. 41 and 42) exchange-correlation functional mentioned later, μ was set as 0.33. Thus, LC scheme describes exchange interaction by a conventional exchange functional in the short-range region and by a HF exchange integral in the long-range region. On the other hand, conventional hybrid schemes, such as B3LYP, describe exchange interaction by simply mixing conventional exchange functionals and a HF exchange with appropriate mixing ratios, which are independent of distances.

B. Long-range corrected time-dependent density functional theory

In TDDFT calculations, excitation energy ω and corresponding excitation vectors $\mathbf{X}$ and $\mathbf{Y}$ are generally obtained by solving a non-Hermitian eigenvalue equation,[24,25]

$$\begin{pmatrix} \mathbf{A} & \mathbf{B} \\ \mathbf{B} & \mathbf{A} \end{pmatrix}\begin{pmatrix} \mathbf{X} \\ \mathbf{Y} \end{pmatrix} = \omega \begin{pmatrix} \mathbf{1} & \mathbf{0} \\ \mathbf{0} & -\mathbf{1} \end{pmatrix}\begin{pmatrix} \mathbf{X} \\ \mathbf{Y} \end{pmatrix}, \tag{7}$$

where $\mathbf{X}$ and $\mathbf{Y}$ are excitation vectors, which represent excitation and deexcitation components of electronic density change, respectively. The elements of matrices $\mathbf{A}$ and $\mathbf{B}$ are

$$A_{ai,bj} = \delta_{ab}\delta_{ij}(\varepsilon_a - \varepsilon_i) + K_{ai,bj}, \tag{8}$$

and

$$B_{ai,bj} = K_{ai,jb}, \tag{9}$$

where ε_p is the pth Kohn-Sham MO energy. As usual, indices i, j,… and a, b,… label occupied and virtual orbitals, respectively. Matrix element $K_{ai,bj}$ in Eqs. (8) and (9) is given by

$$K_{pq\sigma,rs\sigma'} = (pq\sigma|rs\sigma') - c_x\delta_{\sigma\sigma'}(pr\sigma|qs\sigma') + f_{pq\sigma rs\sigma'}^{\mathrm{xc}}, \tag{10}$$

where p, q,… indicate general MOs, and σ and σ' are spin indices. $(pq\sigma|rs\sigma')$ is a two-electron repulsion integral,

$$(pq\sigma|rs\sigma') = \int\int \psi_{p\sigma}^*(r_1)\psi_{q\sigma}(r_1) \times \frac{1}{r_{12}}\psi_{r\sigma'}^*(r_2)\psi_{s\sigma'}(r_2) d^3r_1 d^3r_2, \tag{11}$$

and c_x is a mixing rate of the HF exchange integral in hybrid functionals. In Eq. (10), $f_{pq\sigma rs\sigma'}^{\mathrm{xc}}$ is a Hessian matrix element of the exchange-correlation energy functional E_{xc} in terms of electron density in adiabatic approximation

$$f_{\sigma\sigma'}^{\mathrm{xc}} = \frac{\delta^2 E_{\mathrm{xc}}}{\delta\rho_\sigma(r_1)\delta\rho_{\sigma'}(r_2)}. \tag{12}$$

This TDDFT formalism is easily expanded to LC-TDDFT. As mentioned in the previous section, exchange energy is divided into short- and long-range parts in the LC scheme. In LC-TDDFT, $K_{pq\sigma,rs\sigma'}$ in Eq. (10) is, therefore, expressed as[30]

$$K_{pq\sigma,rs\sigma'} = (pq\sigma|rs\sigma') - \delta_{\sigma\sigma'}(pr\sigma|qs\sigma)_{\mathrm{LC}} + f_{pq\sigma rs\sigma'}^{\mathrm{xc}}, \tag{13}$$

where $(pq\sigma|rs\sigma')_{\mathrm{LC}}$ is the long-range HF exchange integral in the LC scheme given by

$$(pq\sigma|rs\sigma)_{\mathrm{LC}} = \int \psi_{p\sigma}^*(r_1)\psi_{r\sigma}^*(r_2) \times \frac{\mathrm{erf}(\mu r_{12})}{r_{12}}\psi_{s\sigma}(r_1)\psi_{q\sigma}(r_2) d^3r_1 d^3r_2. \tag{14}$$

This LC exchange integral is calculated with atomic-orbital basis in a Davidson-type subspace algorithm. Computational effort of this exchange integral is totally equivalent with that of conventional HF exchange integral.

The excited-state geometry optimizations based on LC-TDDFT require the corresponding analytical excitation energy gradient. The detailed description of LC-TDDFT analytical energy gradient is given in Ref. 31.

III. COMPUTATIONAL DETAILS

We firstly optimized the ground state (S_0) geometry of DMABN by applying the LC scheme to Becke 1988 exchange[41] (B88x) + one-parameter progressive[42] (OP) correlation [LC-BOP (Ref. 32)] in the Kohn-Sham method. The excited-state geometries were then optimized for LE and CT states by using time-dependent Kohn-Sham (TDKS) method with LC-BOP [LC-TDBOP (Refs. 30 and 31)]. For comparison, hybrid (TD)B3LYP was also applied to the geometry optimizations of DMABN for ground and excited states.

Next, we carried out single-point excitation energy calculations. We calculated vertical excitation energies (i.e., absorption energies) from the optimized S_0 structure and vertical deexcitation energies (i.e., emission energies) from the LE and CT excited states at each optimized structure. For comparison, these vertical (de)excitation energy calculations were examined by the singles and doubles full active symmetry-adapted cluster configuration interaction SAC-CI,[43,44] which is a high-quality *ab initio* excited-state theory, at the optimized geometries of LC-(TD)BOP. Be-

TABLE I. Main bond lengths (in Å), twisting angle τ (in deg), and wagging angle ω (in deg) in the structures of DMABN optimized for the ground (S_0), LE, and CT states by LC-(TD)BOP. For comparison, structures optimized by (TD)B3LYP were also calculated. 6-31G* basis set was used in all calculations. The differences in the optimized bond lengths from those in the observed structure are in parentheses.

	LC-(TD)BOP				(TD)B3LYP			
Parameter	S_0		LE	CT	S_0		LE	CT
N1–C8	1.446	(−0.010)	1.446	1.450	1.454	(−0.002)	1.443	1.439
N1–C1	1.370	(+0.005)	1.368	1.404	1.377	(+0.012)	1.434	1.445
C1–C2	1.408	(+0.008)	1.416	1.447	1.418	(+0.018)	1.399	1.419
C2–C3	1.379	(+0.009)	1.420	1.363	1.385	(+0.015)	1.440	1.370
C3–C4	1.395	(+0.007)	1.407	1.417	1.406	(+0.018)	1.402	1.440
C4–C5	1.431	(+0.004)	1.430	1.415	1.429	(+0.002)	1.433	1.400
C5–N2	1.162	(+0.017)	1.163	1.167	1.165	(+0.020)	1.167	1.180
τ	0		20	90	0		38	90
ω	0		0	25	0		0	2

sides, these vertical (de)excitation energies were also evaluated by using pure B88x + Lee-Yang-Parr correlation[45] (BLYP) and hybrid B3LYP.

To investigate solvent effects, we carried out single-point TDKS calculations with a polarizable continuum model[46] (PCM-TDDFT) of acetonitrile solvent. We used a conductorlike model for PCM.[47] In PCM calculations, the static dielectric constant and optical analog were set as 36.64 and 1.806, respectively. The solvent radius was given to be 2.155 Å.

As the basis set, we used 6-31G* in all geometry optimizations and 6-311G^{**} in all single-point energy calculations including PCM-TDDFT and SAC-CI calculations. All TDDFT processes were implemented and executed on GAMESS program[48] and all SAC-CI calculations were performed on GAUSSIAN 03 program.[49]

IV. RESULTS AND DISCUSSIONS

A. Optimized structures of S_0, LE, and CT states

Table I lists the optimized structures of DMABN for ground (S_0), LE, and CT states by LC-(TD)BOP. The optimized structures by (TD)B3LYP are also shown for comparison. All geometry optimizations were carried out with no symmetrical constraint even for the excited states (LE and CT). For the S_0 structures of both LC-BOP and B3LYP, the differences in the optimized bond lengths from the observed x-ray diffraction structure in the crystalline phase[14] are shown in parentheses. The numbering of atoms and the twisting angle τ follow those in Fig. 1. The wagging angle ω is defined as the angle N1–C1–C4 in this figure.

1. Optimized S_0 structure

As we can see from Table I and Fig. 2(a), LC-BOP and B3LYP gave totally planar structures with the twisting angle $\tau=0°$ and the wagging angle $\omega=0°$ for S_0 state. This result is consistent with the experimental results such as microwave spectra ($\tau=0°$),[7] rotationally resolved fluorescence spectra ($\tau=0°$, $\omega=\pm1°$),[50] and manypast theoretical calculations.[51] The optimized bond lengths of LC-BOP showed better agreement with the experimental results[14] than those of B3LYP. The averaged error of LC-BOP structure in bond lengths is 0.006 Å, while the averaged error of B3LYP structure is 0.012 Å. From this result, we may say that LC-BOP gave more accurate S_0 geometry than B3LYP. The largest error of the LC-BOP structure from the experimental value is +0.017 Å for the bond length of C5–N2. For C5–N2 bond, B3LYP also gave a large error (+0.020 Å).

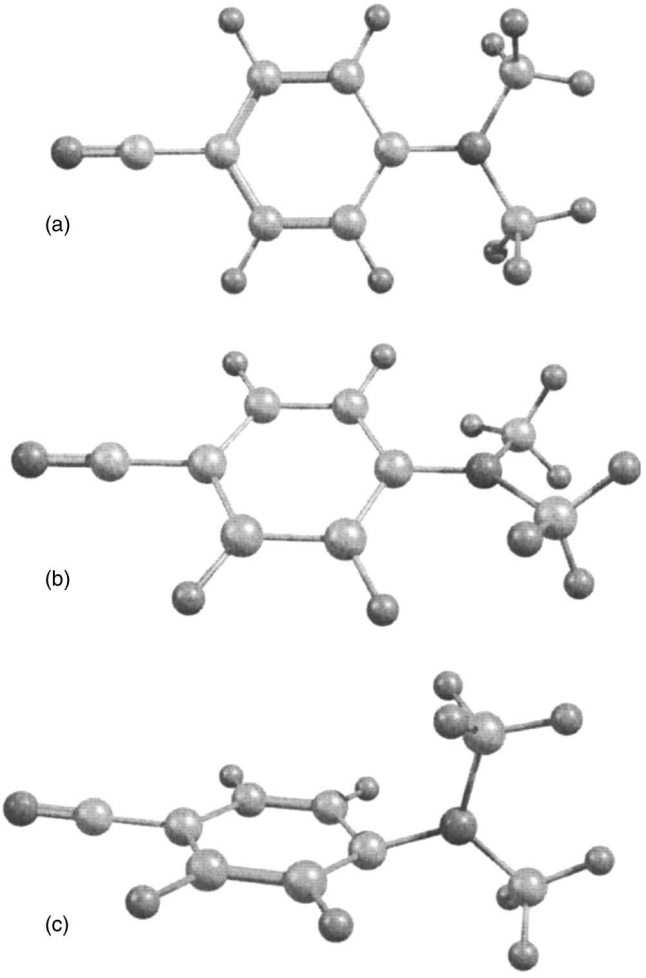

FIG. 2. Optimized structures of the S_0 (a), LE (b), and CT (c) states of DMABN. LC-(TD)BOP was used in the geometry optimizations.

TABLE II. Calculated absorption and emission energies of DMABN in eV. Calculated oscillator strengths are also attached in parentheses. 6-311G** basis set was used in all calculations. All energy calculations were carried out using the geometries optimized LC-TDBOP with 6-31G* basis set.

	In gas phase				In acetonitrile solvent			
	LE		CT		LE		CT	
	Absorption energies at the optimized S_0 state geometry							
(PCM-)LC-TDBOP	4.76	(0.03)	5.05	(0.57)	4.69	(0.06)	4.65	(0.93)
(PCM-)TDB3LYP	4.49	(0.03)	4.74	(0.52)	4.39	(0.05)	4.33	(0.84)
(PCM-)TDBLYP	4.09	(0.02)	4.40	(0.46)	3.96	(0.04)	3.98	(0.72)
SAC-CI	4.62	(0.03)	5.39	(0.62)	···	···	···	···
Expt.	4.25[a]	(0.03)	4.56[a]	(0.68)	···		4.26[b]	
	Emission energies from LE and CT at the corresponding optimized excited-state geometries							
(PCM-)LC-TDBOP	4.20	(0.03)	3.04	(0.00)	4.17	(0.05)	2.87	(0.00)
(PCM-)TDB3LYP	3.93	(0.03)	2.40	(0.00)	3.86	(0.02)	2.20	(0.00)
(PCM-)TDBLYP	3.52	(0.02)	1.71	(0.00)	3.44	(0.02)	1.51	(0.00)
SAC-CI	4.02	(0.05)	3.56	(0.00)	···	···	···	···
Expt.	3.76[c]		3.05[d]		3.44[b]		2.66[b]	

[a]Reference 52.
[b]Reference 53.
[c]Reference 54.
[d]In toluene solvent (Ref. 55).

2. Optimized LE state structure

When no symmetrical constraints were imposed on geometry optimizations, the S_1 optimized structure corresponding to the LE state proceeded to a local minimum of S_1 potential energy surface (PES) from the vicinity of the equivalent planar structure. For this LE state, LC-TDBOP estimated 20° and 0° as the twisting τ and wagging ω angles, respectively [see Table I and Fig. 2(b)]. This result may be consistent with experimental studies, analyses of microwave ($\tau=\sim30°$ and $\omega=\sim0°$),[7] time-of-flight mass ($\tau=\sim30°$),[60] resonant enhanced two-photon ionization ($\tau=26°$),[61] and rotationally resolved fluorescence spectra ($\tau=25°$ and $\omega=3°$).[50] The equilibrium bond lengths of this excited state were not given in these studies. TDB3LYP also gave a reasonable twisting angle $\tau=38°$ in the present constraint free calculation. This twisting angle of TDB3LYP is a little different from the result by Rappoport and Furche with C_2 symmetry constraint ($\tau=33°$). We should notice that the LE potential energy curve is quite shallow for the twisting angle as mentioned later [see Sec. IV C]. Therefore, the twisting angle τ may change quite easily in the LE state due to the shallow potential with respect to the twisting. Table I also indicates that there are remarkable differences between the ground and LE geometries in the bond lengths of the benzene ring. The C2–C3 bond of the benzene ring was stretched by about from the S_0 to LE minima (by 0.041 Å for LC-TDBOP and by 0.055 Å for TDB3LYP). The most remarkable difference between LC-TDBOP and B3LYP was found in the N1–C1 bond (i.e, N–Ph bond): TDB3LYP gave a considerable stretch from S_0 to LE minima by 0.057 Å, although this bond was shortened by 0.002 Å for LC-TDBOP. This difference may come from the rate of the long-range exchange interaction, and it may significantly take part in the twisting of DMABN.

3. Optimized CT state structure

The S_1 optimized structure corresponding to the CT excited state was obtained as the global minimum of S_1 PES with the twisting angle $\tau=90°$. As shown in Table I and Fig. 2(c), LC-TDBOP gave the wagging angles as $\omega=25°$ for the CT optimized structure. In contrast, TDB3LYP gave an insignificant wagging angle (2°.) for this state. This may indicate that the wagging angle of DMABN, which has been suggested in several *ab initio* calculations, is due to the long-range exchange interaction. Similar to the LE state mentioned above, the optimized N1–C1 (i.e., N–Ph) bond length of LC-TDBOP, 1.404 Å, is much shorter than that of TDB3LYP, 1.445 Å. For C–C bond lengths in the benzene ring, LC-TDBOP results were quite different from TDB3LYP ones with the maximum difference of about 0.04 Å. This is in contrast to the ground state structure, for which the maximum difference in bond lengths was about 0.01 Å. This result may suggest that long-range exchange interaction is much more important in excited states than those in ground states.

It is interesting to note that the optimized wagging angles of LE and CT states may have significant implications on investigations into the dual fluorescence mechanism. Zachariasse *et al.* suggested a hypothesis that the dual fluorescence of DMABN is induced by the wagging mode due to vibronic coupling between LE and CT states.[10] This hypothesis has been theoretically denied, because the dual fluorescence obviously occurs through the twisting mode from an energetic point of view.[11] However, the different wagging angles of LE and CT states, 0° and 25° by LC-TDBOP, indicate that wagging mode coupling may also play a certain role in the dual fluorescence mechanism.

B. Absorption and emission energies

Table II summarizes calculated absorption energies from

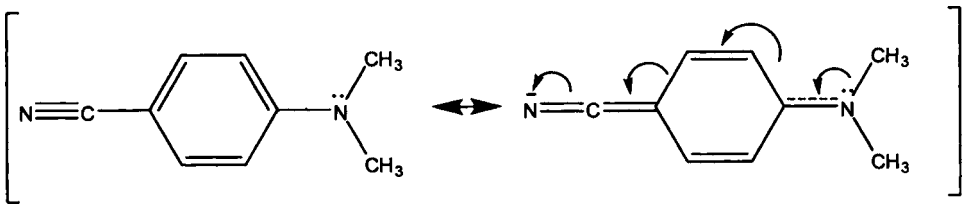

FIG. 3. A possible resonance structure of the ground state of DMABN.

the S_0 minimum of DMABN and emission energies from the LE and CT minima of DMABN. The corresponding oscillator strengths are shown in parentheses. Experimental values are also shown for comparison.[4,52–55] As the solvent effect, a C-PCM model[47] of acetonitrile solvent was used in the calculations of single-point excitation energies and corresponding oscillator strengths.

1. Absorption energies from the S_0 structure

To evaluate the absorption energies from the ground state to LE and CT states, we calculated vertical excitation energies and corresponding oscillator strengths at the optimized S_0 structure. As shown in Table II, LC-TDBOP overestimated the absorption energies for both LE and CT excitations in comparison with the experimental values. Rappoport and Funche reported that TDB3LYP produced good absorption energies both for LE and for CT excitations.[29] To investigate this overestimation, we calculated vertical excitation energies and corresponding oscillator strengths by *ab initio* SAC-CI method and TDDFT with hybrid B3LYP and pure BLYP, at the optimized S_0 structure of LC-BOP (Table II). We used 6-311G** basis set in all these calculations. The SAC-CI method is an *ab initio* highly correlated single-configurational theory including all single and double excitations. We may say that the SAC-CI method is one of the most reliable theories for excited-state calculations. As a result, SAC-CI calculations also overestimated the absorption energies (4.62 eV for LE, 5.39 eV for CT) as well as those of LC-TDBOP (4.76 eV for LE, 5.05 eV for CT). This is in contrast to TDB3LYP and TDBLYP energies. As previously reported,[29] TDB3LYP results (4.40 and 4.67 eV) showed good agreement with experimental values (4.25 and 4.56 eV).

We guess that this discrepancy may come from the resonance structure of the planar ground state. Figure 3 illustrates an expected resonance structure for the planar ground state of DMABN. For such a resonance structure, it is known that doubly excited configurations are partly mixed in the ground state. It is, therefore, presumed that single-configurational theories including TDDFT and SAC-CI slightly overestimate excitation energies for systems containing a resonance ground state structure, because these methods consequently neglect excitations from the mixed high-level doubly excited configurations. To make sure this presumption, we carried out CASSCF(8,8) calculations using 6-31G* basis set at the optimized ground state geometry of LC-BOP. Consequently, we found that the ground state of DMABN partly contains doubly excited configurations, which seem to correspond to the resonance structure in Fig. 3. Therefore, it is highly possible that the accurate absorption energies of TDB3LYP come from an error cancellation.

To evaluate the solvent effect on absorption energies, we calculated vertical excitation energies by LC-TDBOP using PCM for acetonitrile solvent (PCM-LC-TDBOP). The calculated absorption energies are given in Table II. The table shows that the CT state is energetically lower than the LE state in acetonitrile solvent, despite the former is about 0.3 eV higher than the latter in gas phase. This energy inversion by the solvent effect of acetonitrile was suggested in previous theoretical studies.[56,57] Since the calculated oscillator strength of the CT excitation also increases to 0.93, which is much higher than the LE one (0.06), it is presumed that electronic excitations of DMABN in acetonitrile mostly proceed to the CT state in the vicinity of the ground state structure.

2. Emission energy from the LE state

Next, we calculated the vertical deexcitation energy from the LE state and corresponding oscillator strength at the optimized LE structure of LC-TDBOP. In Table II, calculated LE emission energy in gas phase is given with the oscillator strength in parentheses. As the table shows, LC-TDBOP overestimated the LE emission energy in comparison with the experimental result. To investigate this overestimation, we calculated LE emission energies by various theories at the optimized LE geometry of LC-TDBOP. Calculated LE emission energies and corresponding oscillator strengths of these theories are also shown in Table II. In this table, we found that high-level SAC-CI method gave higher emission energy than the experimental. Since TDB3LYP also gave a higher energy, which is closer to SAC-CI energy, TDB3LYP might give a correct LE emission energy provided the resonance effect would be taken into account.

To investigate the emission from the LE state in acetonitrile solvent, we calculated the LE emission energy by taking the solvent effect into consideration. As a result, we obtained almost the same emission energy (4.17 eV) as the energy in gas phase (4.20 eV). Therefore, this result suggests that solvent effect hardly contributes to the LE emission energy. At first glance, this result seems to disagree with previous experimental results, because the assigned peak of LE emission is fairly shifted by the solvent effect: 3.76–3.44 eV in an absorption spectroscopy study. However, we guess that the present result is consistent with this spectroscopy result as mentioned in Sec. IV C.

3. Emission energy from the CT state

For elucidating the CT emission, we also calculated vertical excitation energy and corresponding oscillator strength by various theories at the optimized CT structure of LC-TDBOP. At the optimized CT structure, CT excitation mainly consists of highest occupied molecular orbital (HOMO) to

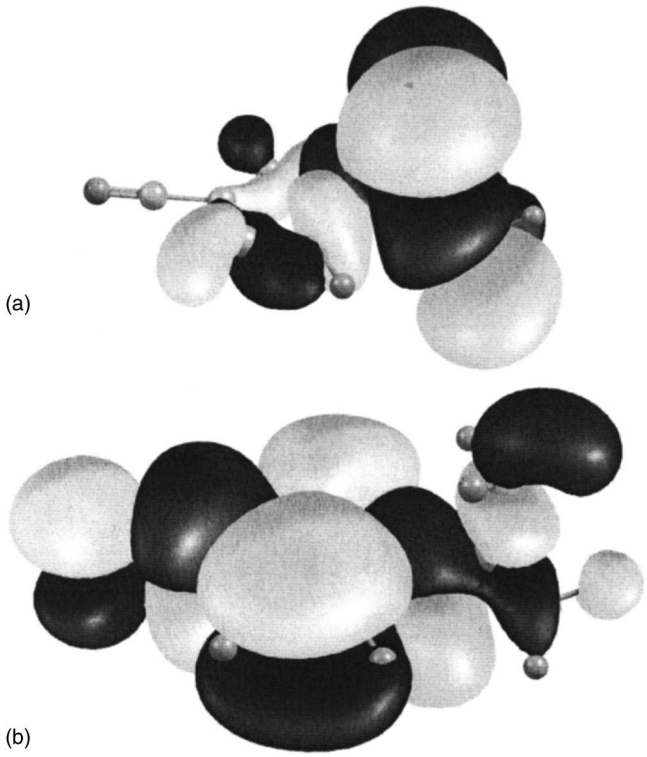

FIG. 4. HOMO (a) and LUMO (b) of DMABN at the optimized CT state structure. LC-TDBOP was used in the geometry optimization.

lowest unoccupied molecular orbital (LUMO) transition. HOMO and LUMO images are illustrated in Fig. 4. This figure clearly shows that the electron transfer proceeds from $N(Me)_2$ group to Ph–CN group. Calculated CT emission energies and oscillator strengths are displayed in Table II. As the table indicates, LC-TDBOP (3.04 eV) showed excellent agreement with the observed emission energy (3.05 eV). In contrast, TDB3LYP and TDBLYP showed significant underestimation in emission energies (2.40 and 1.71 eV, respectively) compared to SAC-CI and experimental results (3.56 and 3.05 eV, respectively). We guess that this result may be originated from the break of resonance structure by the twisting and wagging of DMABN. As shown in Fig. 3, the resonance structure of DMABN seems to be planar due to the C1–N1 double bond. It is, therefore, presumed that the accurate CT emission energy of LC-TDBOP may be due to the single-configurational character of the ground state of DMABN for the twisted structure. On the other hand, the underestimated energies of TDB3LYP and TDBLYP may indicate that the long-range exchange correction is required for usual functionals in TDDFT to reproduce this CT emission energy. In addition, all calculations gave negligible oscillator strengths for the CT emission, despite considerable strengths were given for the CT absorption. This may cause the long-lived high fluorescence of DMABN.

We also calculated the CT emission energy with the solvent effect of acetonitrile. Consequently, PCM-LC-TDBOP gave accurate CT emission energy in acetonitrile solvent, which is close to the experimental value, 2.66 eV. Similar to the gas phase case, the resonance structure may be broken by the twisting and wagging of DMABN. This argument is supported by the underestimated emission energies of PCM-TDB3LYP and PCM-TDBLYP. In acetonitrile solvent, the CT emission gave no oscillator strengths (0.00). Therefore, the long-lived high fluorescence is expected for DMABN in acetonitrile solvent. As shown in Table II, the calculated oscillator strength of the CT excitation (0.00) at the optimized twisted structure was larger than that of the LE state (0.03), although the CT excitation has much larger oscillator strength near the planar structure as mentioned later. This result indicates that the CT emission has a very long lifetime than the LE emission.

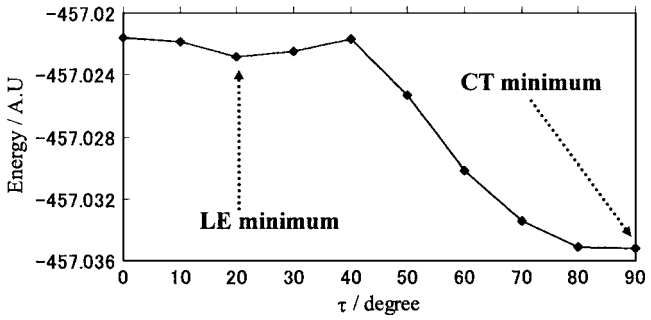

FIG. 5. The S_1 potential energy curve in terms of the twisting angle τ ($\tau=0°-90°$). The geometries were optimized for S_1 state with fixing τ at each angle for 0°–90° and $\omega=0°$.

C. The mechanism of fluorescence

1. Potential energy surface, dipole moment, and oscillator strength in gas phase

To investigate the fluorescence mechanism of DMABN, we draw the potential energy curves of S_1 states in terms of the twisting angle τ ($\tau=0°-90°$) in Fig. 5. For each τ, we carried out geometry optimizations of the S_1 state with fixing τ at each angle for 0°–90° and $\omega=0°$. There are two minima in the S_1 potential curve, which corresponds to the LE minimum ($\tau\sim20°$) and the CT minimum ($\tau=90°$). From this figure, we could see that twisting motion plays a crucial role in dual fluorescence of DMABN.

Besides, we calculated the potential energy curve of the S_2 state at the S_0 geometries with each τ. We should notice that the geometry optimization of the S_2 state was not carried out, because the S_2 state smoothly fell into the S_1 state through the optimization due to the mixing of LE and CT states. This may be because LE and CT states are strongly correlated with each other, if no symmetrical constraint was imposed on the geometry optimizations. To separate LE and CT states, Rappoport and Funche imposed C_2 symmetry in the optimizations of the excited-state geometries.[29] However, separating LE and CT artificially may cause an artificial effect on the potential energy curve. Instead, we used the calculated dipole moments [Fig. 7(a) to assign the dominant character of each state as LE or CT. That is, larger dipole moment points were assigned to the CT state and smaller dipole moment points to the LE state. By assigning the plots of S_1 and S_2 as LE or CT by using dipole moment, we draw the potential curve of LE and CT [Fig. 6(a)]. For comparison, the potential curve of S_0 energy with optimized S_0 structure is also shown. Corresponding oscillator strengths are

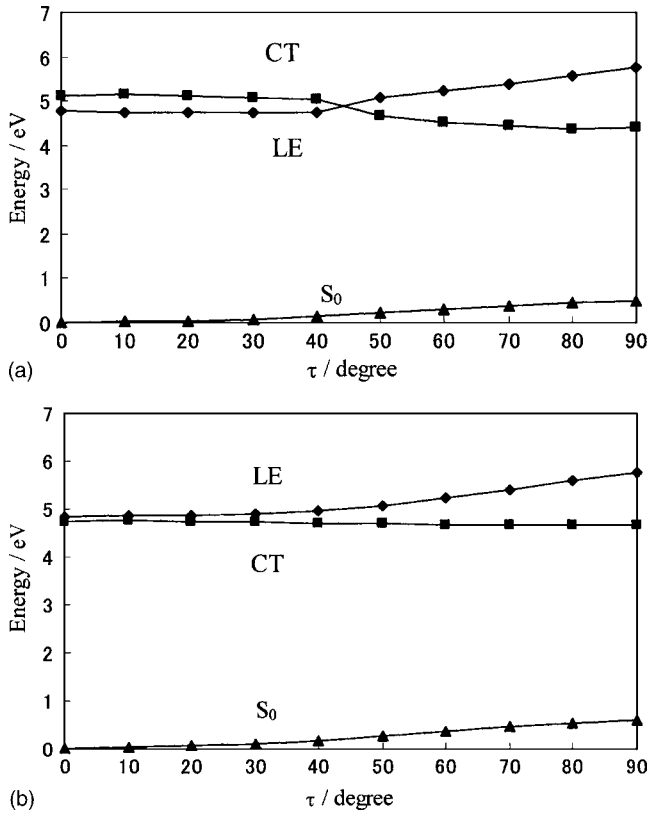

FIG. 6. The potential energy curves of LE and CT states in gas phase (a) and in acetonitrile solvent (b) in terms of the twisting angle τ (τ =0°–90°). The S_1 state energies were determined by the geometry optimizations, and the S_2 state energies were estimated by the single-point excitation energy calculations at the optimized ground state (S_0) structure of LC-BOP at each τ. The optimized S_0 energies are also shown for comparison.

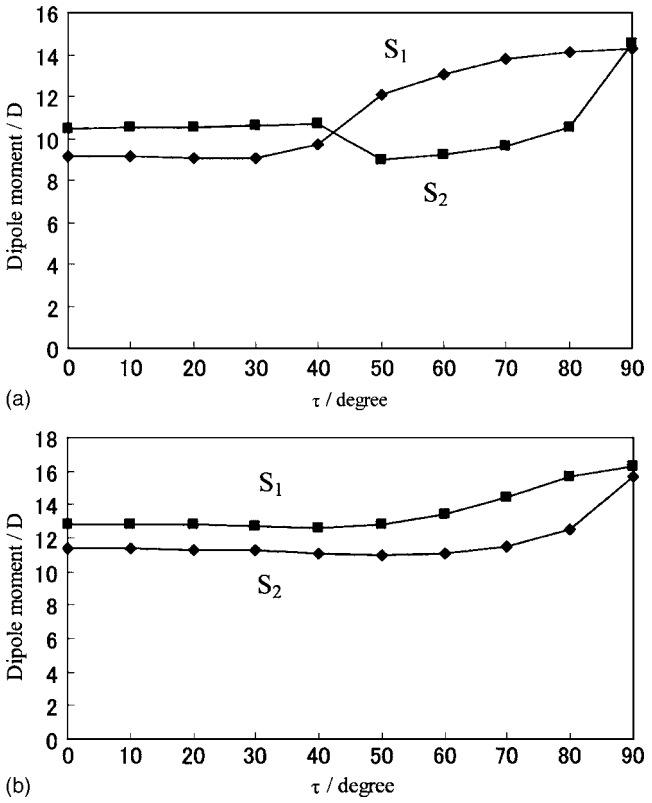

FIG. 7. Calculated dipole moments of S_1 and S_2 states in gas phase (a) and in acetonitrile solvent (b) in terms of the twisting angle τ (τ=0°–90°). The dipole moments of the S_1 and S_2 states were calculated for the optimized S_1 and S_0 geometries, respectively.

also shown in Fig. 8(a). Figure 6(a) shows that the LE state is the lowest excited state at the ground state structure near the planar structure and has a potential energy crossing with the CT state at around τ=45° in gas phase. It was experimentally observed that DMABN emits a single fluorescence in gas phase at room temperature.[53] We suggest that this single fluorescence may be due to the strong vibronic coupling between LE and CT states. According to the calculated oscillator strengths in Fig. 8(a), it is supposed that the photoabsorption chiefly proceeds to the CT (S_2) state in the vicinity of the ground state structure. However, a short-axis polarized spectrum corresponding to the LE fluorescence was detected in fluorescence spectra.[53] It may indicate that the CT (S_2) state rapidly relaxes to the LE (S_1) state due to the strong vibronic coupling. Figure 8(a) also indicates that the CT fluorescence may be yielded if the absorption proceeds at a large twisting angle over 45°. Since the ground state of DMABN has a shallow potential energy for the twisting angle, it is expected that the large angle may be easily given by the increase of temperature. Actually, jet-cooled fluorescence spectra showed that DMABN emits the dual fluorescence in gas phase at high temperature, 383 K.[58]

2. Potential energy surface, dipole moment, and oscillator strength in acetonitrile

Next, we calculated S_1 and S_2 potential energy surfaces [Fig. 6(b)], dipole moments [Fig. 7(b)], and oscillator strengths [Fig. 8(b)] in acetonitrile solvent by PCM-LC-TDBOP. Since we have no energy gradient for PCM-LC-TDBOP, S_0 optimized geometries with each τ were used. Figure 6(b) indicates that the CT state is the lowest excited state for all twisting angles in acetonitrile solvent. As shown in Fig. 8(b), the calculated oscillator strength of the CT excitation is much higher than that of the LE excitation. These results seem to be inconsistent with the fluorescence spectrum of DMABN that shows a dual fluorescence containing a major peak and a plateau secondary peak in acetonitrile solvent at room temperature.[53] However, the minor peak is only a plateau shoulder of the major peak of CT emission. It is interesting to note that Zachariasse recently gave an important comment on the fluorescence spectrum of DMABN in acetonitrile from an experimental point of view.[53,59] Referring to a previous polarization spectroscopic analysis,[1] he pointed out that short-axis polarization, which may correspond to LE fluorescence, was only detected at the blue edge of the spectrum and the minor peak corresponding to LE emission was mainly polarized in the direction of the long axis.[59] According to this observation, we propose that the secondary peak of the dual fluorescence in acetonitrile is only a plateau shoulder of CT emission. In Fig. 8(b), we found the rapid decrease of oscillator strengths for the CT excitation as the twisting angle increases from τ=40° to 90°. However, the number of CT states may increase for the twisting angle, because the CT state energy declines monotonically from τ=40° to 90° [Fig. 6(b)]. Since the number of emitting photons is in proportion to the multiplication of

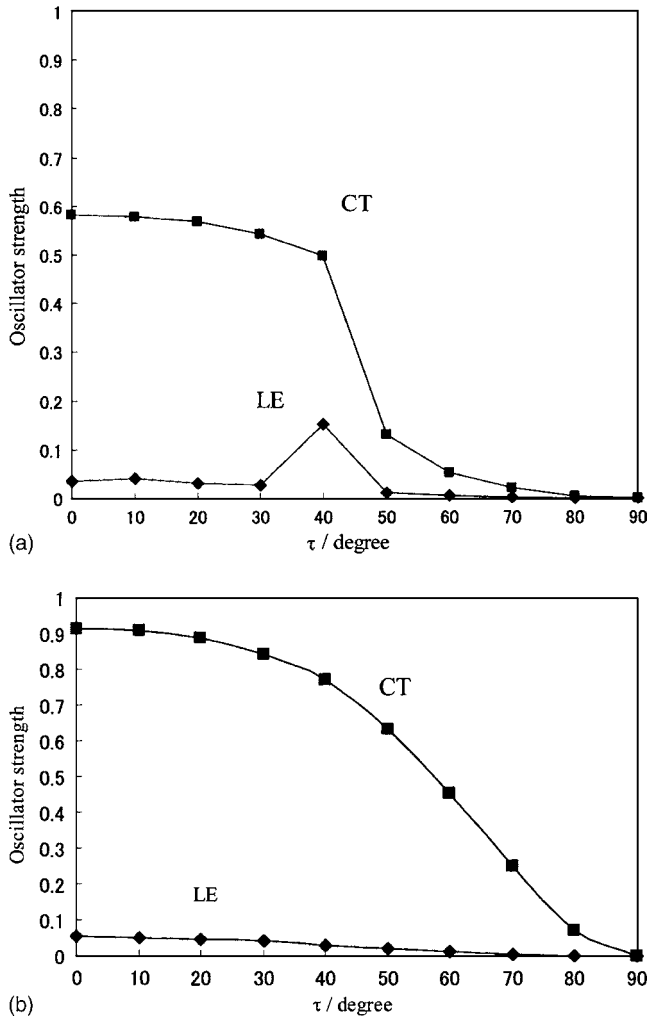

FIG. 8. Calculated oscillator strengths of LE and CT states in gas phase (a) and in acetonitrile solvent (b) in terms of the twisting angle τ (τ =0°–90°).

oscillator strength and number of states, we presumed that the spectrum height may plateau for the increase in the twisting angle, i.e., for the decrease in excitation energy. We guess that this unique feature may cause the misinterpretation of this peak.

3. Fluorescence mechanism in gas phase and acetonitrile at room temperature

As we can see from Table II and Fig. 6(a), it is presumed that the photoabsorption chiefly proceeds to the S_2 state (CT) in both gas phase and acetonitrile solvent due to the high oscillator strength. However, a "normal" LE emission was experimentally observed in gas phase at room temperature.[1] As experimentally suggested,[58] this may come from an internal conversion from CT to LE states due to a strong vibronic coupling between these states through the twisting process. Based on this argument, we suggest a fluorescence mechanism of DMABN in gas phase at room temperature as follows.

(1) The photoabsorption mainly proceeds to the CT (S_2) state near the planar structure ($\tau = \sim 0°$).
(2) The CT (S_2) state of DMABN brings about the internal conversion to the LE (S_1) state by the strong vibronic coupling between CT and LE states through the twisting mode.
(3) After relaxing to the LE minimum near the planar structure, a single fluorescence is emitted from the LE state.

On the other hand, in acetonitrile solvent at room temperature, the CT state is stabilized to the S_1 state for whole angles, as shown in Fig. 6(b). Furthermore, the oscillator strength of the CT excitation is much higher than that of the LE excitation and the LE state is easily relaxed to the CT state because of the vibronic coupling mentioned above. Considering above-mentioned Zachariasse's observation,[59] we suggest a new fluorescence mechanism of DMABN in acetonitrile solvent at room temperature as follows.

(1) The photoabsorption mostly proceeds to the CT (S_1) state.
(2) The main redshifted fluorescence is radiated from the CT state in the twisted structure (τ=90°).
(3) The secondary fluorescence is only a plateau shoulder of CT emission.

V. CONCLUSIONS

In this study, we theoretically investigated the dual fluorescence of 4,4′-dimethylaminobenzonitrile (DMABN) by performing analytical excited-state geometry optimizations using long-range corrected time-dependent density functional theory (LC-TDDFT).[31,32] In several previous calculations,[31,32] we have already confirmed that LC-TDDFT gives accurate charge transfer energies with maintaining its accuracy in valence excitation energy calculations. By using the analytical energy gradient of LC-TDDFT, we investigated the unique fluorescence mechanism of DMABN, which is significantly different from gas phase to polar solvent conditions.

First, we optimized the geometries of ground (S_0), locally excited (LE), and charge transfer (CT) states by the analytical energy gradient of LC-(TD)BOP with no symmetrical constraint. As a result, we found that LC-BOP gave a planar structure for the S_0 state with accurate bond lengths, which are very close to the experimental ones. The optimized planar structure is supported by previous experimental and theoretical results.[7,51] For the LE state, LC-TDBOP gave a certain twisting angle (τ=20°) and no wagging angle (ω =0°). The optimized twisting and wagging angles are consistent with the results of various spectroscopic analyses.[7,50,60,61] Furthermore, LC-TDBOP gave 90° twisted structure with the wagging angle (ω=25°) for the CT state. Since the LE state has no wagging angles, this result may evoke the hypothesis of Zachariasse *et al.*[10] that the dual fluorescence of DMABN is induced by the wagging mode due to the vibronic coupling between LE and CT states.

Next, we calculated absorption energies from the optimized S_0 geometry and two different emission energies from the optimized LE and CT geometries. LC-TDBOP calcula-

tions were performed with and without the solvent effect of acetonitrile. As a result, we found that LC-TDBOP overestimated the absorption energies for both LE and CT excitations. However, we also found that the *ab initio* SAC-CI calculation using the optimized LC-TDBOP geometry overestimated these absorption energies as well. We supposed that this overestimation may come from the resonance planar structure of the ground state. Actually, we found that the doubly excited configurations, which correspond to the resonance structure, were mixed in the ground state in a CASSCF calculation.

We also calculated the LE and CT emission energies and corresponding oscillator strengths with and without solvent effect at the optimized structures of LC-TDBOP. As a result, we found that the solvent effect hardly contributes to the LE emission energy. This result may conflict with the previous arguments on the observed fluorescence, which has been assigned to be the LE emission, because this fluorescence is fairly shifted by the solvent effect. For the CT emission, LC-TDBOP gave very accurate emission energy, despite other TDDFTs clearly underestimated this energy. We guessed that this may come from the break of the resonance structure due to the twisting and wagging of DMABN, because the resonance structure of DMABN seems to have a planar structure. For the oscillator strengths, we found that the CT excitation gave infinitesimal oscillator strength. This result indicates that the redshifted fluorescence would be long lived.

Finally, we explored the fluorescence mechanism of DMABN in gas phase and in acetonitrile solvent by calculating potential energy curves, dipole moments, and oscillator strengths. Calculated results clearly indicated that the photoabsorption of DMABN chiefly proceeds to the CT state in both situations due to its large oscillator strength. For the process after the photoabsorption in gas phase, we suggested that the CT state is converted to the LE state due to the strong vibronic coupling of LE and CT states; and consequently, DMABN emits the single fluorescence from the LE state near the planar structure. On the other hand, we found that the CT state is the lowest excited state over all twisting angles in acetonitrile solvent. This result seems inconsistent with previous spectroscopy analyses showing the dual fluorescence, in which the main peak was assigned to CT emission and the secondary peak was assigned to LE emission in acetonitrile solvent at room temperature.[53] However, we concluded that the secondary peak, which gives a plateau shoulder in the main peak, may also come from the CT fluorescence. This is because the oscillator strength of the CT excitation rapidly decreases to zero as the twisting angle increases. That is, this spectrum may have been misinterpreted, because the spectrum height does not grow steadily for the decrease of the excitation energy. This hypothesis is supported by Zachariasse's observation on a polarization spectroscopy that the short-axis polarization was detected only at the blue edge of this minor spectrum and this spectrum was mainly polarized in the direction of the long axis.[59]

In summary, the fluorescence mechanism of DMABN is explained as follows.

In gas phase at room temperature,

(1) the photoabsorption mainly proceeds to the CT (S_2) state near the planar structure ($\tau = \sim 0°$).
(2) The CT (S_2) state of DMABN brings about the internal conversion to the LE (S_1) state by the strong vibronic coupling between CT and LE states through the twisting mode.
(3) After relaxing to the LE minimum near the planar structure, a single fluorescence is emitted from the LE state.

On the other hand, in acetonitrile solvent at room temperature,

(1) the photoabsorption mostly proceeds to the CT (S_1) state.
(2) The main redshifted fluorescence is radiated from the CT state in the twisted structure ($\tau = 90°$).
(3) The secondary fluorescence is only a plateau shoulder of CT emission.

ACKNOWLEDGMENTS

The authors would like to thank Professor Shigehiko Hayashi of Kyoto University for his helpful discussions. This research was supported by the Core Research for Evolutional Science and Technology (CREST) of the Japan Science and Technology Corporation (JST). It was also supported in part by a contribution from Hitachi Chemical Co., Ltd.

[1] E. Lippert, W. Lüder, F. Moll, W. Nügele, H. Boss, H. Prigge, and I. Seibold-Blaakensten, Angew. Chem. **73**, 695 (1961).
[2] J. Platt, J. Chem. Phys. **17**, 484 (1949).
[3] K. Rotkiewicz, K. H. Grelllmann, and Z. R. Grabowski, Chem. Phys. Lett. **19**, 315 (1973).
[4] E. M. Kosower, and H. Dodiuk, J. Am. Chem. Soc. **98**, 924 (1976).
[5] Z. R. Grabowski, K. Rotkiewicz, A. Siemiarczuk, D. J. Cowley, and W. Baumann, Nouv. J. Chim. **3**, 443 (1979).
[6] U. Leinhos, W. Kühule, and K. A. Zachariasse, J. Phys. Chem. **95**, 2013 (1991).
[7] O. Kajimoto, H. Yokoyama, Y. Ooshima, and Y. Endo, Chem. Phys. Lett. **179**, 455 (1991).
[8] Y. P. Sun, M. A. Fox, and K. P. Johnston, J. Am. Chem. Soc. **114**, 1187 (1992).
[9] W. Schuddeboom, S. A. Jonker, J. M. Warman, U. Leinbos, W. Kühule, and K. A. Zachariasse, J. Phys. Chem. **96**, 10809 (1992).
[10] K. A. Zachariasse, T. von der Haar, A. Hebecher, U. Leinhos, and W. Kühule, Pure Appl. Chem. **65**, 1745 (1993).
[11] L. Serrano-Andrés, M. Merchán, B. O. Roos, and R. Lindh, J. Am. Chem. Soc. **117**, 3189 (1995).
[12] A. L. Sobolewski and W. Domcke, Chem. Phys. Lett. **259**, 119 (1996).
[13] A. L. Sobolewski, W. Sudholt, and W. Domcke, J. Phys. Chem. A **102**, 2716 (1998).
[14] A. Heine, R. Herbst-Irmer, D. Stalke, W. Kühule, and K. A. Zachariasse, Acta Crystallogr., Sect. B: Struct. Sci. **B50**, 363 (1994).
[15] D. Majumdar, R. Sen, K. Bhattacharyya, and S. P. Bhattacharyya, J. Phys. Chem. **95**, 4324 (1991).
[16] A. B. J. Parusel, G. Köhler, and S. Grimme, J. Phys. Chem. A **102**, 6297 (1998).
[17] A. B. J. Parusel, G. Köhler, and M. Nooijen, J. Phys. Chem. A **103**, 4056 (1999).
[18] A. B. J. Parusel, Phys. Chem. Chem. Phys. **2**, 5545 (2000).
[19] B. Mennucci, A. Toniolo, and J. Tomasi, J. Am. Chem. Soc. **122**, 10621 (2000).
[20] A. B. J. Parusel, W. Rettig, and W. Sudholt, J. Phys. Chem. A **106**, 804 (2002).
[21] N. Minezawa and S. Kato, J. Phys. Chem. A **109**, 5445 (2005).
[22] B. O. Roos, in *Ab Initio Methods in Quantum Chemistry*, edited by K. P.

Lawley (Wiley, New York, 1987), pp. 399–446.
[23] K. Andersson, P. A. Malmquist, and B. O. Roos, J. Chem. Phys. **96**, 1218 (1992).
[24] R. Bauernschmitt and R. Ahlrichs, Chem. Phys. Lett. **256**, 454 (1996).
[25] R. E. Stratmann, G. E. Scuseria, and M. J. Frisch, J. Chem. Phys. **109**, 8218 (1998).
[26] F. Jensen, *Introduction to Computational Chemistry* (Wiley, New York, 2001).
[27] F. Furche and R. Ahlrichs, J. Chem. Phys. **117**, 7433 (2002).
[28] A. D. Becke, J. Chem. Phys. **98**, 5648 (1993).
[29] D. Rappoport and F. Furche, J. Am. Chem. Soc. **126**, 1277 (2004).
[30] Y. Tawada, T. Tsuneda, S. Yanagisawa, and K. Hirao, J. Chem. Phys. **120**, 8425 (2004).
[31] M. Chiba, T. Tsuneda, and K. Hirao, J. Chem. Phys. **124**, 144106 (2006).
[32] H. Iikura, T. Tsuneda, T. Yanai, and K. Hirao, J. Chem. Phys. **115**, 3540 (2001).
[33] T. Leinenger, H. Stoll, H.-J. Werner, and A. Savin, Chem. Phys. Lett. **275**, 151 (1997).
[34] W. Kutzelnigg, J. Mol. Struct.: THEOCHEM **768**, 163 (2006).
[35] R. van Leeuwen and E. J. Baerends, Phys. Rev. A **49**, 2421 (1994).
[36] D. J. Tozer, J. Chem. Phys. **112**, 3507 (1999).
[37] T. Yanai, D. P. Tew, and N. C. Handy, Chem. Phys. Lett. **393**, 51 (2004).
[38] M. Kamiya, T. Tsuneda, and K. Hirao, J. Chem. Phys. **117**, 6010 (2002).
[39] T. Sato, T. Tsuneda, and K. Hirao, J. Chem. Phys. **123**, 104307 (2005).
[40] M. Kamiya, H. Sekino, T. Tsuneda, and K. Hirao, J. Chem. Phys. **122**, 234111 (2005).
[41] A. D. Becke, Phys. Rev. A **38**, 3098 (1988).
[42] T. Tsuneda, T. Suzumura, and K. Hirao, J. Chem. Phys. **110**, 10664 (1999).
[43] H. Nakatsuji, Chem. Phys. Lett. **59**, 362 (1978).
[44] H. Nakatsuji and K. Hirao, J. Chem. Phys. **68**, 2053 (1978).
[45] C. Lee, W. Yang, and R. G. Parr, Phys. Rev. B **37**, 785 (1988).
[46] M. Cossi and V. Barone, J. Chem. Phys. **115**, 4708 (2001).
[47] V. Barone and M. Cossi, J. Phys. Chem. A **102**, 1995 (1998).
[48] M. W. Schmidt, K. K. Baldridge, J. A. Boatz *et al.*, J. Comput. Chem. **14**, 1347 (1993).
[49] M. J. Frisch, G. W. Trucks, H. B. Schlegel *et al.*, GAUSSIAN 03, Gaussian Inc., Pittsburgh, PA, 2003.
[50] A. E. Nikolaev, G. Myszkiewicz, G. Berden, W. Leo Meerts, J. F. Pfanstiel, and D. W. Pratt, J. Chem. Phys. **122**, 084309 (2005).
[51] S. Kato and Y. Amatatsu, J. Chem. Phys. **92**, 7241 (1990).
[52] C. Bulliard, M. Allan, G. Wirtz, E. Haselbach, K. A. Zachariasse, N. Detzer, and S. Grimme, J. Phys. Chem. A **103**, 7766 (1999).
[53] K. A. Zachariasse, M. Grobys, and E. Tauer, Chem. Phys. Lett. **274**, 372 (1997).
[54] U. Lommatzsch, A. Gerlach, C. Lahmann, and B. Brutschy, J. Phys. Chem. A **102**, 6421 (1998).
[55] Y. V. Il'ichev, W. Kühnle, and K. A. Zachariasse, J. Phys. Chem. A **102**, 5670 (1998).
[56] R. Cammi, B. Mennucci, and J. Tomasi, J. Phys. Chem. A **104**, 5631 (2000).
[57] B. Mennucci, A. Toniolo, and J. Tomasi, J. Am. Chem. Soc. **122**, 10621 (2000).
[58] R. Howell, D. Phillips, H. Pitek, and K. Yoshihara, Chem. Phys. **188**, 303 (1994).
[59] K. A. Zachariasse, Chem. Phys. Lett. **320**, 8 (2000).
[60] V. H. Grassian, J. A. Warren, E. R. Bernstein, and H. V. Secor, J. Chem. Phys. **90**, 3994 (1989).
[61] H. Saigusa, N. Miyakoshi, C. Mukai, T. Fukagawa, S. Kohtani, and R. Gordon, J. Chem. Phys. **119**, 5414 (2003).